Nanoscale Advances

ROYAL SOCIETY OF CHEMISTRY

PAPER

Cite this: *Nanoscale Adv.*, 2020, **2**, 2387

Fulleropyrrolidine-functionalized ceria nanoparticles as a tethered dual nanosystem with improved antioxidant properties†

Alessandra Pinna,[a] Eleonora Cali,[a] Gwilherm Kerherve,[a] Grazia Galleri,[b] Michele Maggini,[c] Plinio Innocenzi [d] and Luca Malfatti *[d]

Dual-tethered nanosystems which combine different properties at the nano scale represent a new fascinating frontier of research. In the present work, we present an example of a dual nanosystem designed to enhance the radical scavenging performances. Fulleropyrrolidine has been bonded to cerium oxide nanoparticles (nanoceria) to form a dual tethered system. Fulleropyrrolidine, bearing a silyl-alkoxide group, has been chemically bonded to the nanoceria surface, providing unprecedented antioxidant activity. This effect has been evaluated using an L929 mouse fibroblast cell line exposed to UV light. The fulleropyrrolidine molecules tethered to nanoceria enhance the radical scavenging properties of the oxide. At the same time, fulleropyrrolidine mitigates the potential toxicity of nanoceria at high doses. On the other hand, cerium oxide nanoparticles provide a strong hydrophilicity to the dual nanosystem, ensuring the administration in a cellular environment and preventing macroscopic aggregation of fulleropyrrolidine. The rational assembly of two different components in one nanosystem appears as a promising route for the development of "smarter" medical and cosmetic devices.

Received 17th January 2020
Accepted 12th April 2020

DOI: 10.1039/d0na00048e

rsc.li/nanoscale-advances

Introduction

Cerium oxide nanoparticles have been gaining increasing attention because of their UV-shielding and radical scavenging properties.[1–6] Cerium oxide is a semiconductor with a wide band gap capable of strong absorption in all the three regions of UV light (UV-A, B, and C, respectively).[7] Cerium oxide, synthesized in the form of nanoparticles, shows autocatalytic activity, due to the Ce atoms being able to switch between the 3+ and 4+ oxidation states.[8] This property has put cerium oxide nanoparticles in the spotlight because the autocatalytic activity leads to a strong radical-scavenging effect when this phenomenon occurs in a biological environment at pH 7.4. Several research groups have reported the beneficial effects of nanoceria when applied to cardio-, neuro-protective and radiation therapies[9] or the prevention of retinal degeneration induced by reactive oxygen species (ROS).[10–12] Despite the promising applications, the use of nanoceria in biomedicine is still controversial.[13]

The autocatalytic effect, under particular conditions, can turn nanoceria from a radical scavenger to a radical former.[14] This can make nanoceria at high doses a toxic drug for several types of cells, converting the nanoparticles into a carcinogenic compound.[15] At present, the administration dose and the nanoparticle size seem to be crucial parameters to modulate the nanoceria response when it is used in a biological environment. Larger particles tend to produce radicals while smaller particles are more prone to neutralize these species.[16–18] The reasons for this dual behaviour lie in the relative amount of Ce^{3+} and Ce^{4+} on the nanoparticle surface. A full design of the system properties, therefore, requires extremely accurate control of their size,[19] with an error smaller than a nanometer. This explains why the use of nanoceria as a drug for medical therapies would be difficult without using surface functionalization or core–shell structures.

On the other hand, fullerene-based materials have proved to be an efficient radical scavenger when exposed to UV, X- or even γ-rays.[20] Fullerene molecules can attract and neutralize 20 or more free radicals per molecule with better performances than vitamin C and vitamin E. The radical scavenging effect is due the conjugated double bonds of the molecule. The low-lying lowest unoccupied molecular orbital (LUMO) can easily accept an electron from the reacting radicals. The radical scavenging

[a]Department of Materials, Imperial College London, South Kensington Campus, London, SW72BP, UK
[b]Department of Clinical and Experimental Medicine, University of Sassari, 07100, Sassari, Italy
[c]Department of Chemical Sciences, University of Padova, 35131, Padova, Italy
[d]Department of Chemistry and Pharmacy, CR-INSTM, University of Sassari, 07100, Sassari, Italy. E-mail: luca.malfatti@uniss.it

† Electronic supplementary information (ESI) available: Raman spectrum of the substrate, TEM images of CeO_2 nanoparticles, DLS of Si-Fulp/ceria, SI-Fulp and ceria in ethanol, details about the calculation method for determining the weight percentage of Si-Fulp in the dual nanosystem and the ratio of Si-Fulp molecules with respect to ceria nanoparticles, images of Si-Fulp/ceria and ceria solutions after 3 months from the synthesis, NMR ^{1}H ^{13}C and MALDI-TOF spectra of fulleropyrrolidine. See DOI: 10.1039/d0na00048e

process appears to be catalytic, allowing the fullerene to react with many superoxides without being consumed. Due to this property, fullerenes have been defined as radical sponges.[21,22] This property envisages that fullerene and its derivatives (such as fulleropyrrolidine) could be successfully applied to prevent sensitive materials from UV-degradation and biological tissues from ROS overproduction.[23,24] In previous years, the antiviral activity of fullerenes has been extensively investigated and directly correlated with the unique anti-oxidant properties of its molecular structure.[25] Aqueous C_{60} suspensions, for instance, have shown to protect the liver of rodents against free-radical damage, without causing acute or subacute toxicity.[26]

In this work, we have designed a tethered dual nanosystem capable of merging the radical scavenging properties of the cerium oxide nanoparticles and fullerene derivative. We have used fulleropyrrolidine bearing an ethoxy-silyl group to increase the solubility of the fullerene in an aqueous environment and enable the functionalization of inorganic materials, as shown in previous work.[27]

This new system is expected to mitigate the eventual risk coming from the use of naked cerium oxide nanoparticles. The functionalization of cerium oxide nanoparticles with functional molecules, in fact, has already proved to be a successful strategy in both cosmetic and medical applications.[28] Nanoceria, for instance, has been functionalized with branched polyethylenimine and then reacted with genipin (a natural molecule extracted from *Gardenia jasminoides*) to formulate a cosmetic made of pigmented nanoparticles with improved free radical scavenging activity.[29] Ceria nanoparticles, functionalized with dextran and loaded with curcumin, have been capable of inducing substantial cell death in neuroblastoma cells.[30] Finally, Prussian Blue-functionalized nanoceria has been applied in the ultrasensitive detection of the tumour necrosis factor-α.[31] All these applications, however, make use of a polymer to coat the nanoparticles. After this step a second functional species, such as a molecule or a dye, is attached.

In our work, nanoceria has been functionalized with fulleropyrrolidine, bearing an alkoxy-silyl group, through a chemical bond. This functionalization provides partial solubility of the fullerene molecules and ensures close proximity to the ceria nanoparticle surface. The tethered dual nanosystem has been characterized and tested as a protecting device against a UV insult for a specific type of cell line, an L929 mouse fibroblast. The combination of two distinct types of nanomaterials to form multifunctional nanodevices is an innovative strategy. This approach would allow the development of medical applications and a new generation of cosmetics with improved efficacy.

Results and discussion

Efficient protection against UV light by the ceria–fulleropyrrolidine (Si-Fulp/ceria) system relies on an effective functionalization of nanoceria with the organic molecules. To achieve this goal, we have used silylated fulleropyrrolidine bearing three terminal ethoxide groups. These functions have been at first hydrolyzed by acid catalysis in ethanol to form –OH groups and then reacted with the OH–Ce of the nanoceria surface to induce polycondensation. Fig. 1 shows the diagram of the overall reaction.

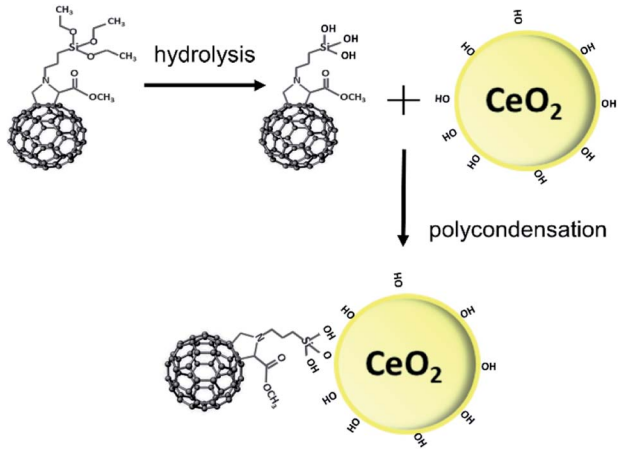

Fig. 1 Diagram of nanoceria functionalization with Si-Fulp.

Although the polycondensation reactions can also occur among different Si-Fulp molecules, after several purification cycles, we have observed a clear change in the colour of nanoceria. The pale-yellow nanoceria solution turned into light brown after functionalization. To assess the structure and composition of the system, we have used a combination of different characterization techniques. Raman spectroscopy, in particular, has been used to assess the functionalization of the nanoceria surface with Si-Fulp. Fig. 2 shows the Raman spectra in the 1700–150 cm^{-1} range of nanoceria, Si-Fulp, and Si-Fulp/ceria.

The Raman spectrum of bare nanoceria deposited onto a silicon wafer (Fig. 2, blue line) exhibits an asymmetric band at 464 cm^{-1} which is assigned to the symmetric breathing mode of the Ce–O vibrational unit in crystalline cerium oxide with a cubic fluorite structure.[32,33] The band peaked at 1049 cm^{-1} has

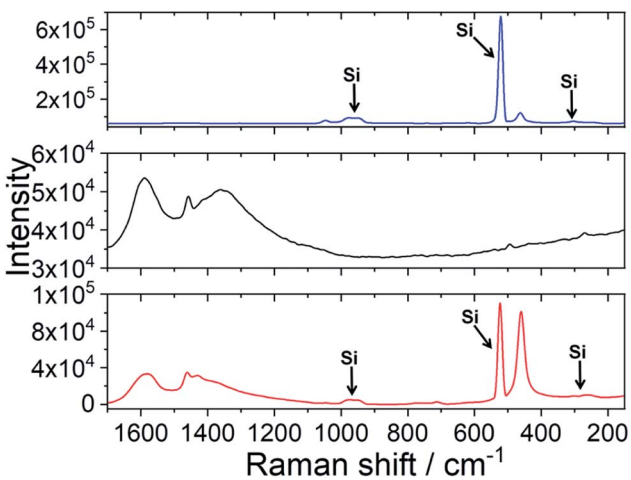

Fig. 2 Raman spectra in the 1700–150 cm^{-1} range of nanoceria (blue line), the pristine Si-Fulp (black line) and nanoceria functionalized with Si-Fulp (red line). The bands at 303, 523 and 965 cm^{-1} are due to the monocrystalline silicon substrate.

been attributed to residual and unreacted $CeNO_3$ used as a nanoceria precursor.[34] The dimension of ceria crystallites (D) has been estimated by using the Full-Width Half Maximum (FWHM) of the band at 464 cm^{-1} by applying the following formula:[35]

$$\text{FWHM } (cm^{-1}) = 10 + \frac{124.7}{D}$$

By this method, the dimension of ceria nanoparticles was calculated to be 10.8 nm. The other bands, which appear in the spectrum (303, 523 and 965 cm^{-1}), are due to the monocrystalline silicon substrate (see the ESI, Fig. S1†). The spectrum of Si-Fulp (Fig. 2, black line) is characterized by three absorption bands peaking at 1431 cm^{-1} $H_g(7)$; 1456 cm^{-1}, $A_g(2)$; and 1581 cm^{-1}, $H_g(8)$, which are associated to the stretching mode of the cages of C_{60}.[36] The Si-Fulp/ceria spectrum (Fig. 2, red line) shows both signals of nanoceria and Si-Fulp suggesting the successful functionalization of the cerium oxide nanoparticles. Compared with the pure Si-Fulp spectrum, the Raman bands related to C_{60} in the Si-Fulp/ceria spectrum are slightly shifted to a lower wavelength by 3 cm^{-1}. The shift is attributed to the strong interaction between nanoceria and the chemically grafted Si-Fulp.[37]

Fig. 3 shows the XRD patterns relative to nanoceria (blue line), Si-Fulp (black line), and the Si-Fulp/ceria (red line). Nanoceria shows the typical diffraction pattern of face-centered cubic CeO_2 (JCPDS no. 34-0394), with the fluorite structure. [(111), (200), (220), (311), (222), (400), (331), and (420) planes at $2\theta = 28.5$, 33.1, 47.5, 56.3, 59.1, 69.4, 76.7, 79.1, 88.4, and 95.3°]. The crystallite dimension, as calculated by using the Scherrer equation, was found to be ≈7.8 ± 0.4 nm. This size is compatible with TEM measurements of naked nanoceria (see the ESI, Fig. S2†). The Si-Fulp XRD pattern corresponds to a crystallized face-centred cubic lattice of C_{60} with the diffraction planes (111), (220), (311), (222), (331), (420), (442) and (333) at 10.6, 12.3, 17.5, 20.6, 24.5, 27.2, 27.9, 30.7, and 32.5 2θ angles.[38] Finally, the pattern of Si-Fulp/ceria only shows the diffraction peaks attributed to cerium oxide, proving that no residual Si-Fulp crystals remained after functionalization and purification.

The high-resolution TEM (HR-TEM) image in Fig. 4a reveals the self-assembly of Si-Fulp into amorphous aggregates when reacted with nanoceria in water. The Fast Fourier Transform (FFT) of the TEM image (Fig. 4a) has confirmed the cubic nature of the crystalline nanoceria with an average size of ≈7 nm. An interplanar spacing of $d = 0.19$ nm, corresponding to the (220) plane, was measured.

The Si-Fulp covers the cerium oxide nanoparticle surface, as shown in Fig. 4a, and an amorphous layer surrounds a small aggregate of nanoparticles. Cid *et al.* have, in fact, demonstrated the capability of fullerene-based structures to self-organize into different shapes as a function of the dispersing solvent.[39] Furthermore, the aggregates in the dark field STEM image of Fig. 4b clearly show a difference in contrast due to the change in the material composition. The bright (and therefore denser) regions correspond to the crystalline nanoceria; the darker aggregate surrounding nanoceria corresponds to the amorphous self-assembled Si-Fulp. Fig. 4d–g show the elemental distribution of the Si-Fulp/ceria (the selected area in Fig. 4c). The analysis confirms the functionalisation of nanoceria with Si-Fulp. In particular, EDS measurements have confirmed that the amorphous aggregate visible in the selected area of Fig. 4c is fulleropyrrolidine grafted on the nanoceria surface (C map, Fig. 4e). The fullerene compound is bound to the nanoceria

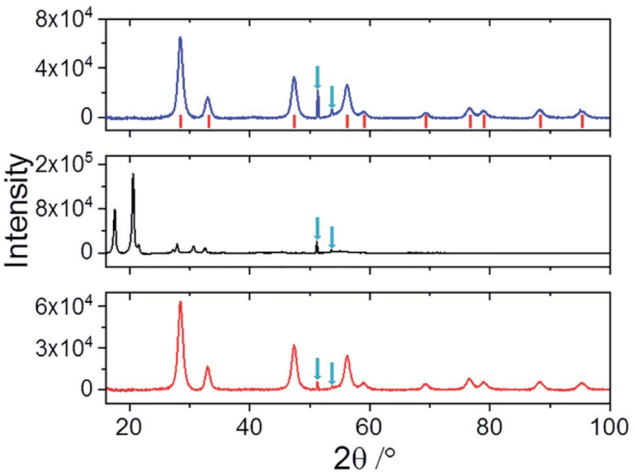

Fig. 3 XRD patterns of nanoceria (blue line), Si-Fulp (black line) and Si-Fulp/ceria (red line) in the 15–100 2θ range. The red ticks show the standard diffraction peaks of fluorite CeO_2 (JCPDS no. 34-0394). Nanoceria crystallite dimension was calculated by using the Scherrer equation considering the diffraction peaks at 2θ 28, 33 and 47°. The sharp diffraction peaks (down arrows) at 51.3 and 53.6° in 2θ are due to the silicon substrate.

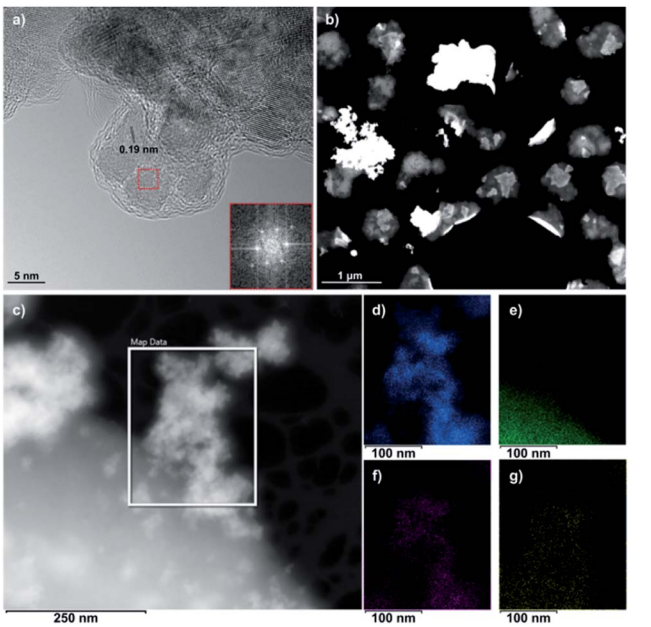

Fig. 4 (a) HR-TEM and (b) DF-STEM images of Si-Fulp/ceria. The inset in (a) shows the FFT image obtained of nanoceria (red-boxed region) with a d-spacing of 0.19 nm. (c) Transmission electron image of Si-Fulp/ceria. EDS elemental maps of (d) Ce, (e) C, (f) O, and (g) Si obtained in the boxed region in (c).

particles aggregate (Ce and O maps, Fig. 4d and f) through the silanol tail (Si map, Fig. 4g).

The aggregation state of the Si-Fulp-grafted nanoceria has also been studied by dynamic light scattering. The measures show that the ceria nanoparticle and Si-Fulp in ethanol have an average size of the aggregates of 47.18 ± 11.52 and 323 ± 63.42 nm, respectively. After functionalization, the Si-Fulp-grafted nanoceria aggregates increase in size with an average value of 619.7 ± 116 nm. The size distribution plots of the three samples are reported in the ESI, Fig. S3.† Both Si-Fulp/ceria and nanoceria remain stable in aqueous solutions for long time. Fig. S4 (ESI)† shows a picture of the two solutions after 3 months from the synthesis.

The concentration of Ce^{3+} and Ce^{4+} has been evaluated in both species by using XPS. Fig. 5a shows the Ce 3d core level of nanoceria and Si-Fulp/ceria. In the case of nanoceria, six peaks are observed, namely v, v″, v‴, u, u″ and u‴. They are attributed to the tetravalent form of Ce in CeO_2 and with a spin orbit splitting of ~18.5 eV.[40–43] After functionalization of nanoceria with Si-Fulp, two shoulders appear at 884.9 eV (v′) and 903.4 eV (u′) corresponding to the satellite peaks of the Ce 3d in its trivalent form.[40,43] This clearly suggests that the functionalisation of Si-Fulp promotes the formation of the Ce^{3+} site at the surface of the ceria nanoparticles. Fig. 5b and c show a detailed view of the deconvoluted Ce 3d spectra used to calculate the concentration of Ce^{3+} and Ce^{4+}. The concentration of Ce^{3+} increases from 31% to 43% in bare bone nanoceria and Si-Fulp/ceria, respectively, while Ce^{4+} decreases from 69% to 57%. It was observed that nanoceria can act both as superoxide dismutase (SOD), by neutralizing superoxide radicals, and catalase (CAT), by promoting the decomposition of hydrogen peroxide into water and oxygen.[44] According to the literature, an increase in Ce^{3+}/Ce^{4+} ratio induces mimetic properties to Si-Fulp/ceria which are more similar to SOD than CAT.[44]

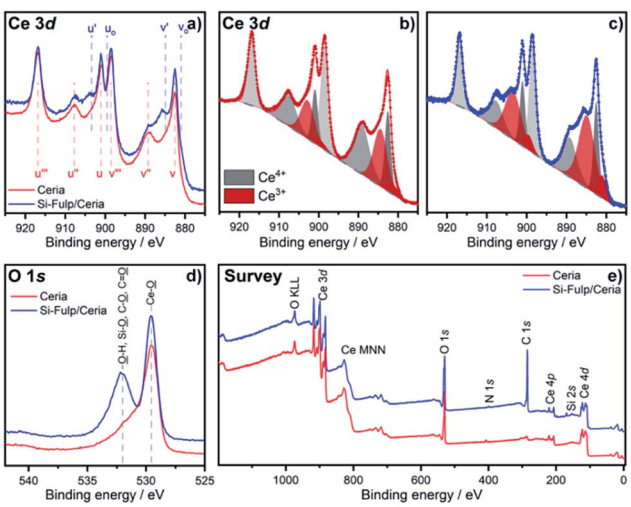

Fig. 5 (a) Ce 3d spectra of the bare nanoceria (red) and Si-Fulp/ceria (blue). For comparison, both samples were normalised to the peak noted (u‴) at B.E. of 916.8 eV. Deconvoluted Ce 3d spectra of the (b) bare nanoceria and (c) Si-Fulp/ceria. (d) O 1s spectra and (e) survey spectra of the bare nanoceria (red) and Si-Fulp/ceria (blue).

The O 1s spectrum of (Fig. 5d) shows the onset of the band picked at 532 eV, when nanoceria is functionalised with Si-Fulp. This band is related to the presence of the OH group on the nanoceria surface whereas the other band at 530 eV is attributed to lattice oxygen.[45] Ce^{3+} ions, which are mostly present at the nanoceria surface, are active sites for the reaction.[46] In particular, in aqueous solution, the cerium ions can act as catalytic sites for H_2O dissociation, resulting in the formation of –OH surface groups.[47] The OH group is capable of forming strong Ce–O–Si– bonds with silicate ions (–Ce–OH + –Si–O– ↔ –Ce–O–Si– + OH^-).[48] The XPS data clearly proved nanoceria surface functionalization with Si-Fulp through oxygen bonds. The survey scan (Fig. 5e), measured from 0 to 1200 eV, has shown binding energies assigned to cerium, oxygen, silicon, carbon and nitrogen. This indicates the purity of the samples.

The amount of Si-Fulp grafted onto nanoceria has been estimated by thermogravimetric analysis (TGA) of nanoceria, Si-Fulp, and Si-Fulp/ceria (Fig. 6). The blue line shows the multistage thermal decomposition of nanoceria; the first step (198 °C) corresponds to the urea conversion into liquid ammonia isocyanic acid (HNCO) while the second (303 °C) is related to the rapid vaporization of ammonia as a consequence of HNCO hydrolysis.[49] In the range between 370 and 600 °C, the mass loss is attributed to the conversion of residual $Ce(OH)_3$, which is on the nanoceria surface, into CeO_2.[50]

The thermogravimetric curve of Si-Fulp (Fig. 6, black line) shows a first weight loss (531 °C) assigned to the decomposition of alkoxides which is in the functionalization group of fulleropyrrolidine.[51] The second weight loss, occurring from 535 to 865 °C, is assigned to the structural degradation of fulleropyrrolidine, in agreement with previous findings.[52] The multistage decomposition of Si-Fulp/ceria particles is a combination of the features shown by the two previous materials, *i.e.* nanoceria and Si-Fulp (Fig. 6, red line). The weight loss of Si-Fulp/ceria has enabled the calculation of the weight% of Si-Fulp bound to nanoceria, which was found to be 4.7%. Furthermore, considering the average size of nanoceria and the density of cerium dioxide, the ratio between the Si-Fulp-grafted molecules and the amount of nanoceria can be estimated to be 39.5, indicating that the amount of the fulleropyrrolidine molecules is higher than the number of cerium oxide nanoparticles in the tethered nanosystem. The details of the calculation, as derived from TGA, are available in the ESI.† Although the ratio between Si-Fulp-grafted molecules and nanoceria is quite high, we cannot exclude the presence of bare cerium oxide nanoparticles after the functionalization process.

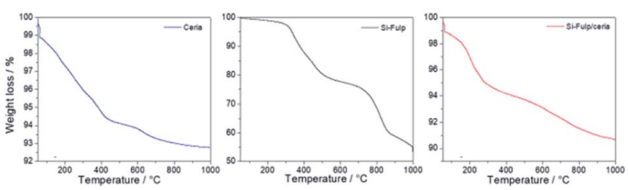

Fig. 6 TGA analysis of nanoceria (blue line), Si-Fulp (black line) and Si-Fulp/ceria (red line) in air at a heating rate of 10 °C min^{-1}.

UV-Visible absorption spectroscopy has been used to assess the functionalization of nanoceria with the Si-Fulp. Fig. 7a shows the typical absorption spectrum of Si-Fulp: the absorption bands peaking at 212, 255 and 321 nm are assigned to the C_{60} dipole-allowed transition[53] while a very weak band at 430 nm, is typical of 1,2-dihydrofullerenes.[54] The spectrum of nanoceria is characterized by two absorption bands, one at 210 nm and a second one at 327 nm corresponding to the Ce 4f–O 2p and Ce 5d–O 2p valence states.[55] The band gap, calculated by the Tauc method, is 3.12 eV. The Si-Fulp/ceria spectrum shows a combination of absorption bands attributed to Si-Fulp and nanoceria with a strong band at 210 nm and a second large band peaked around 300 nm. Si-Fulp/ceria, when dissolved in water, shows a red shift of the absorption bands (250 and 314 nm respectively) which further increases as a function of the solution concentration. Moreover, above 350 nm, we observe an increase in absorbance due to the increase of Ce^{3+} formed during surface functionalization (Fig. 7b).[56,57] The radical scavenging property of fulleropyrrolidine combined with the autocatalytic activity of cerium oxide nanoparticles creates an unprecedented antioxidant effect when the Si-Fulp/ceria nanosystems are dispersed in a liquid environment. This property has been at first tested by using a chemical assay with 2-diphenyl-1-picrylhydrazyl (DPPH) and then confirmed by using an *in vitro* test with L929 mouse fibroblast exposed to a UV insult. The DPPH molecule in water forms a radical with specific absorption at 517 nm.

This allows monitoring the radical scavenging properties of a specific compound by measuring the UV-Visible spectroscopy of the absorbing radical molecule. Fig. 8 shows the change in intensity as a function of time of the 327 and 517 nm absorption bands (0.078 mg mL^{-1} Si-Fulp/ceria concentration). The spectra show a progressive decrease in intensity of the absorption bands with the increase of time.

A similar trend is observed by monitoring the intensity decrease of the 517 nm absorption band as a function of the Si-Fulp/ceria concentration (Fig. 9a, red line, and Fig. 9b). The same experiment has been also performed with bare cerium oxide nanoparticles for comparison (Fig. 9a, blue line). The observed trend suggests that when Si-Fulp is grafted on nanoceria, the percentage of radical inhibition increases about 10%, therefore improving the potential of nanoceria as a radical scavenger. This is due to the mutual effect of Si-Fulp and nanoceria, which are both contributing to the radical scavenging.

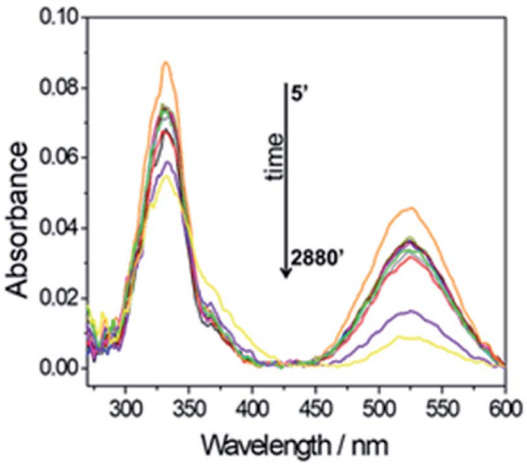

Fig. 8 UV-Vis spectroscopy of a Si-Fulp/ceria dispersed in DPPH water solution (0.078 mg mL^{-1}) as a function of time (min.).

Finally, the antioxidant activity and cytotoxicity of both nanoceria and Si-Fulp/ceria have been evaluated *in vitro* by using a flow cytometry assay using L929 mouse fibroblast cells. L929 cells have been exposed to increasing concentrations of nanoparticles (0.05 mg mL^{-1}, 0.1 mg mL^{-1} and 1.5 mg mL^{-1}) for 24 and 48 hours. After incubation with nanoparticles, the cells were exposed to UV light (λ = 265 nm) for 1 hour to simulate an oxidative insult. The antioxidant protection of both nanoceria and Si-Fulp/ceria against reactive species has been assessed by measuring the viability of the cells after exposure to UV. Fig. 10 shows the average results obtained from these experiments. The top left of Fig. 10 shows no significant difference in apoptosis at 24 h between the control (CTRL) and cells treated with nanoceria at all concentrations. On the

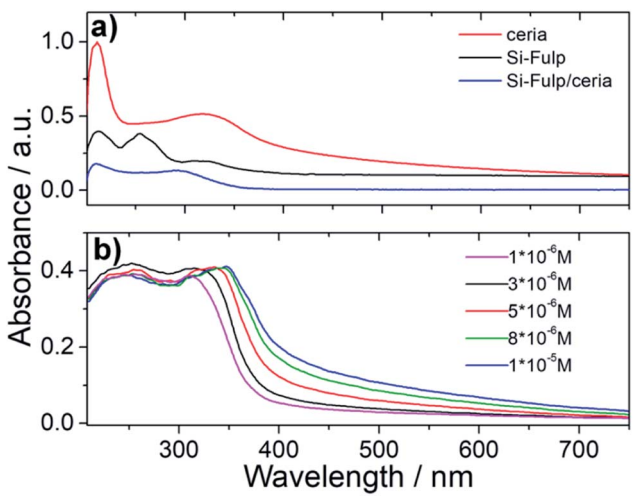

Fig. 7 (a) UV-Vis spectroscopy of nanoceria, Si-Fulp and Si-Fulp/ceria in water. (b) UV-Vis spectra of Si-Fulp/ceria in water at different concentrations.

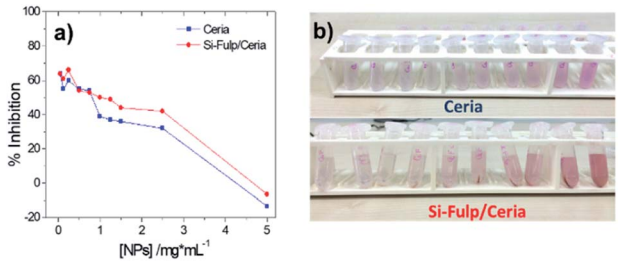

Fig. 9 (a) Change in intensity of the 517 nm band *vs.* nanoceria concentration (blue line) and Si-Fulp/ceria (red line) concentration. (b) Decoloration of nanoceria and Si-Fulp/ceria solutions as a function of the antioxidant concentration.

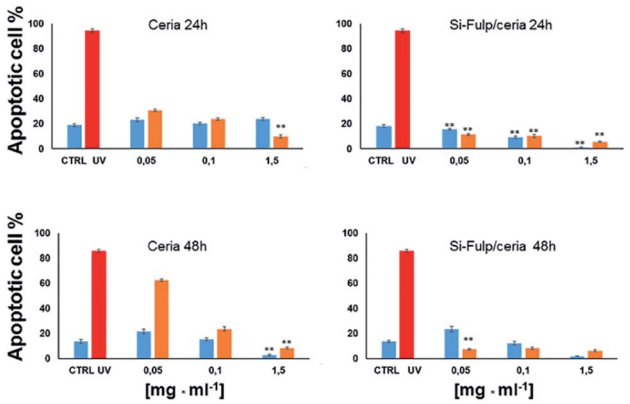

Fig. 10 Bar graphs showing the percentage of apoptotic L929 mouse fibroblast cells *in vitro* treated with different concentrations of nanoceria and exposed to UV irradiation for 24 h (top graphs) and 48 h (bottom graphs). The orange and light blue bars refer to UV-irradiated and not UV-irradiated cells, respectively. The red bar refers to the control, irradiated with UV and not treated with nanoceria. Asterisks indicate statistically significant differences between nanoceria-treated L929 cells *vs.* CTRL ($p < 0.01$).

contrary, the same cells exposed to UV show a significant difference in apoptosis at all nanoceria concentrations with respect to the UV control with $p < 0.001$; the higher the nanoceria concentration, the lower the apoptosis. From these preliminary results we can assess that nanoceria, especially at 1.5 mg mL^{-1}, is capable of protecting the cells from the UV insult.

Moreover, the functionalisation of nanoceria with Si-Fulp (top right Fig. 10) empowers the protective effect at all the used concentrations of the dual-tethered nanosystem against the UV insult. In this second graph the statistical difference ($p < 0.001$) is expressed with a dose-dependent trend both in the exposed (orange bars) and not-exposed (blue bars) cells, with the exception of the sample treated with 0.05 mg mL^{-1} *vs.* CTRL, where no significant difference has been calculated.

In the bottom left of Fig. 10 (ceria 48 h), a significant increase in apoptosis is observed between cells treated with nanoceria (both exposed and not-exposed) and the control ($p < 0.001$). In the cells not-exposed to UV, apoptosis decreases with increasing nanoceria concentration ($p < 0.001$). The presence of Si-Fulp on the nanoceria surface dramatically decreases apoptosis in UV-exposed cells with respect to samples without Si-Fulp (Fig. 10, bottom right). This highlights the ability of the dual-tethered nanosystem to provide greater protection against UV. The reduction of apoptosis is clear at the concentration of 0.05 mg mL^{-1} of ceria–Si-Fulp with mild, but significant, decreases in apoptosis at higher concentrations. On the other hand, by comparing the sample not exposed to the UV insult, we observe no differences in apoptosis between samples treated with Si-Fulp or not-treated. In fact, there is the same significant difference of apoptosis, which is dose-dependent, towards the controls, both with or without Si-Fulp. This evidence suggests that Si-Fulp/ceria is a highly efficient nanosystem to protect against radicals and it is very well tolerated by the L929 cells.

Experimental

Synthesis of nanoceria

Cerium(III) nitrate hexahydrate ($Ce(NO_3)_3 \cdot 6H_2O$, ABCR 99.9%), urea (CH_4N_2O, Aldrich 99%), 2-propanol (99.7%, Carlo Erba), 1 M hydrochloric acid (HCl, Aldrich), 5 M aqueous ammonia (NH_4OH, Aldrich), ethanol (EtOH, Fluka 99.8%), 2,2-diphenyl-1-picrylhydrazyl (DPPH, Aldrich 99%), and methanol (MeOH, Aldrich, 99.8%) were used as received without further purification. Urea was used as a coordinating agent, NH_4OH and $Ce(NO_3)_3$ as inorganic precursors.

7.00 g of $Ce(NO_3)_3 \cdot 6H_2O$ were dissolved in 20 mL of 2-propanol; then 0.5 mL of 1 M HCl were added and stirred until complete dissolution. In a separate vial, 2.00 g of urea were dissolved into 20 mL of 2-propanol containing 0.5 mL of HCl 1 M and stirred for 5 min. The urea solution was then added, dropwise, to the $Ce(NO_3)_3$ solution under stirring, and when the addition was complete, 14 mL of NH_4OH (aq.) were added to the mixture. Afterwards, the solution was exposed to microwaves (4 times at 600 W for 10 s), washed with water and centrifuged at 10 000 rpm. The supernatant was discarded and a light yellow milky pellet (1.12 g CeO_2) was dispersed in 10 mL of water (nanoceria stock suspension, 112 mg mL^{-1}).

Synthesis of alkoxy-silyl-fulleropyrrolidine

Fulleropyrrolidine (Si-Fulp) (Chart 1) was synthesized according to the work of Bianco *et al.*;[58] it was characterized by NMR spectroscopy and MALDI-TOF (see the ESI Fig. S5 and S6†).

Nanoceria functionalization with Si-Fulp (Si-Fulp/ceria)

10 mg of Si-Fulp was dissolved in 750 μL of EtOH and 50 μL of HCl 1 N. The dispersion was sonicated at room temperature until complete dissolution. In a separate vial, 50 mg of nanoceria (450 μL of nanoceria stock suspension) were dispersed in 200 μL of deionized water and mixed with a Si-Fulp solution which was sonicated in an ultrasound bath for 1 hour at 60 °C. Later on, the Si-Fulp/ceria nanoparticles were washed 3 times with water and centrifuged at 5000 rpm. After the third washing step the supernatant was completely transparent, indicating the removal of unreacted Si-Fulp molecules. The supernatant was therefore discarded and the pellet was dispersed in 1 mL of water.

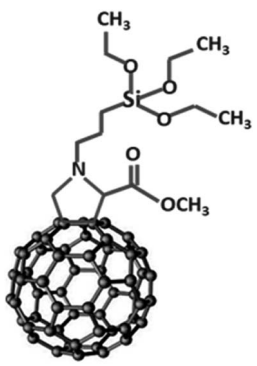

Chart 1

Antioxidant activity

The antioxidant activity of nanoceria and Si-Fulp/ceria was evaluated by using 2,2-diphenyl-1-picrylhydrazyl (DPPH) radical-scavenging assays. DPPH is a free radical, stable at room temperature, which produces a violet solution in methanol. This free radical is reduced in the presence of an antioxidant molecule, giving rise to a colorless methanol solution.

In detail the reaction mixture containing 750 μL of nanoceria and Si-Fulp/ceria aqueous solutions at different concentrations (0.078, 0.195, 0.39, 0.78, 1.17, 1.56, 1.95, 2.34, 3.9, and 7.8 mM) were incubated with 375 μL of DPPH methanol solution (0.05 mM). After 5 minutes the samples were centrifuged at 5000 rpm for another 3 min and the supernatant was measured by using a UV-Vis spectrophotometer at 517 nm fixed wavelength. The mixture of 750 μL of water and 375 μL of MeOH corresponds to the blank while the mixture of 750 μL of water and 375 μL of DPPH is the control. The DPPH decoloration, which is correlated to the scavenging activity (SA%), was calculated by using the following formula using the absorbance (Abs) of the sample and the control:

$$SA\% = [(\text{Abs control} - \text{Abs sample})/\text{Abs control}] \times 100$$

Characterization

The crystalline structure and nanoparticle dimensions were characterized by X-ray diffraction spectroscopy using a Bruker D8 discover instrument in grazing incidence geometry with a Cu Kα line ($\lambda = 1.54056$ Å); the X-ray generator worked at a power of 40 kV and 40 mA. The patterns were recorded in 2θ ranging from 10 to 100° with a step size of 0.05° and a scan speed of 0.5 s in a repetition mode for 12 h until maximization of the signal-to-noise ratio.

A Raman microscope was used to study the functionalization of nanoceria with Si-Fulp. A Bruker Senterra confocal Raman microscope working with a laser excitation wavelength of 532 nm at 12 mW of nominal power was used for optical microscopy (100× magnification) and Raman spectroscopy analysis; the spectra were recorded by averaging 30 acquisitions of 2 s.

Thermogravimetric analysis was performed using a TA Instrument SDT Q600 thermobalance with alumina crucibles. Nanoceria, Si-Fulp, and Si-Fulp/ceria powder were dried at 60 °C for 24 h and placed into the crucibles. The measurements were done using 38.79 mg of nanoceria, 36.72 mg of Si-Fulp/ceria and 2.37 mg of Si-Fulp in a nitrogen flow of 100 mL min^{-1} with a 5 °C min^{-1} heating rate over a temperature range 22–1000 °C.

UV-Visible absorption spectra were recorded using a Nicolet Evolution 300 UV-Vis spectrophotometer working in intelliscan mode; UV-grade silica glass (Heraeus) has been used as background reference.

The aggregate size of nanoceria, Si-Fulp and Si-Fulp/ceria in solution was investigated using Dynamic Light Scattering (DLS, Malvern instrument 2000). Before the DLS measurements, the dried particles were dissolved in ethanol (1.8 mg mL^{-1}) and sonicated in a sonication bath for 30 min.

Moreover, the samples were analysed by transmission electron microscopy (TEM) using a JEOL JEM-2100F TEM operating at a 200 kV voltage and a FEI Titan operating at a 300 kV voltage equipped with a Cs aberration image corrector. The chemical composition of the samples was determined through energy dispersive X-ray spectroscopy (EDS) operated in scanning-transmission electron microscopy (STEM) mode (EDS 80 mm X-Max detector, Oxford Instruments). Specimens for TEM analysis were prepared by sonication of powder samples in DI water which were subsequently drop-cast on holey carbon film copper grids (3.05 mm diam. 300 mesh, TAAB).

The surface chemistry of the nanoceria material was analysed by X-ray Photoelectron Spectroscopy (XPS). XPS spectra were recorded on a Thermo Scientific K-Alpha+ X-ray photoelectron spectrometer operating at 8×10^{-9} mbar base pressure. This system incorporates a monochromated, microfocused Al Kα X-ray source ($h\nu = 1486.6$ eV) and a 180° double focusing hemispherical analyzer with a 2D detector. The X-ray source was operated at 6 mA emission current and 12 kV anode bias providing an X-ray spot size of up to 400 μm^2. Core level spectra were recorded at 20 eV pass energy and surveys at 200 eV pass energy. A flood gun was used to minimize the sample charging that occurs when exposing an insulated sample to an X-ray beam. Deconvolution of Ce 3d spectra was performed using the Casa XPS software. A linear background was subtracted to the data and peaks were fitted using a product of Gaussian and Lorentzian ratio. The binding energy (B.E.) was corrected by aligning the C 1s peak of the adventitious carbon (C–C) at 284.8 eV.

Cell culture

NCTC clone 929 Clone of strain L (also known as L929; ECACC 85011425) were obtained from the European Collection of Authenticated Cell Cultures (London, UK). Cells were cultured as a monolayer in Dulbecco's modified Eagle medium (DMEM, Sigma-Aldrich, USA) containing 2 mM L-glutamine, 10% fetal bovine serum (FBS, Sigma-Aldrich), 20 U penicillin, and 20 μg streptomycin mL^{-1} (Sigma-Aldrich) at 37 °C in a humidified incubator with 5% CO_2.

Cells treatment with nanoparticles

The cells were washed with Dulbecco's phosphate-buffered saline (PBS, Bioshop, UK) and detached from the flask's surface using 0.25% trypsin with 0.02% EDTA (Sigma-Aldrich, Poland). Cells were cultured in a 24 well cell culture tray, and when the cells were 75–80% confluent (approximately 2×10^5 cells per well), they were treated with increasing concentrations of nanoparticles (0.05 mg mL^{-1}, 0.1 mg mL^{-1} and 1.5 mg mL^{-1}) for 24 and 48 hours. After the incubation with nanoparticles, the cells were exposed or not exposed to UV light ($\lambda = 265$ nm) for 1 hour to simulate an oxidative insult. Afterwards L929 cells were detached from the cultured well, washed with PBS and collected in 12 × 75 mm flow cytometric tubes. Subsequently, L929 fibroblast cells were stained with an Annexin V-APC Apoptosis Kit (BD Pharmingen™ Cat no 556547) and with propidium iodide (PI).

Cell apoptosis assay

Annexin V and PI staining were used to quantify the number of apoptotic cells. L929 fibroblast cells were collected and washed twice with PBS. After centrifuging, the cells were resuspended in 500 μL of binding buffer in a flow cytometric tube. Soon after, 5 μL of Annexin V-FITC and 5 μL of PI were added to the cell suspension, mixed well and incubated for 15 min at room temperature in the dark. The stained cells were acquired by FACS Canto (Becton Dickinson, San Jose, USA) flow cytometry and analysed by using Diva Software 6.3.30.000 total events were acquired for each experimental point and the percentage of early and late apoptotic and necrotic cells were analysed with GraphPad Prism 7.0 software.

Conclusions

Combining nanoceria and fulleropyrrolidine properties at the nano scale is a challenging and innovative approach to improve the rational design of functional materials. Fulleropyrrolidine bearing an alkoxy-silyl group is an efficient modifier of the cerium oxide nanoparticle surface, and the Si-Fulp/ceria dual system is a novel class of tethered nanomaterials with improved functionalities. The dispersion of the fulleropyrrolidine molecules is, however, limited by their solubility. The tethered dual nanosystem shows improved antioxidant activity when added to water or biological media containing radical species, although the presence of not-functionalized nanoceria could lead to an underestimate of this effect. In addition, the cytotoxicity of Si-Fulp/ceria is strongly mitigated with respect to high doses of nanoceria. This is a direct result of the coupling with fulleropyrrolidine. Our approach, which involves the rational design of dual systems, tethered at the nanoscale, is a further step towards the development of advanced devices for healthcare and cosmetics.

Conflicts of interest

There are no conflicts to declare.

Acknowledgements

The University of Sassari is acknowledged for funding through "fondo di ateneo per la ricerca 2019".

References

1 H. J. Kwon, D. Kim, K. Seo, Y. G. Kim, S. I. Han, T. Kang, M. Soh and T. Hyeon, Ceria Nanoparticle Systems for Selective Scavenging of Mitochondrial, Intracellular, and Extracellular Reactive Oxygen Species in Parkinson's Disease, *Angew. Chem.*, 2018, **57**, 9408.

2 H. J. Kwon, M.-Y. Cha, D. Kim, D. K. Kim, M. Soh, K. Shin, T. Hyeon and I. Mook-Jung, Mitochondria-Targeting Ceria Nanoparticles as Antioxidants for Alzheimer's Disease, *ACS Nano*, 2016, **10**, 2860.

3 F. Corsi, F. Caputo, E. Traversa and L. Ghibelli, Not Only Redox: The Multifaceted Activity of Cerium Oxide Nanoparticles in Cancer Prevention and Therapy, *Front. Oncol.*, 2018, **8**, 309.

4 S. M. Hirst, A. S. Karakoti, R. D. Tyler, N. Sriranganathan, S. Seal and C. M. Reilly, Anti-inflammatory properties of cerium oxide nanoparticles, *Small*, 2009, **5**, 2848.

5 A. Karakoti, S. Singh, J. M. Dowding, S. Seal and W. T. Self, Redox-active radical scavenging nanomaterials, *Chem. Soc. Rev.*, 2010, **39**, 4422.

6 S. Das, S. Singh, J. M. Dowding, S. Oommen, A. Kumar, T. X. Sayle, S. Saraf, C. R. Patra, N. E. Vlahakis, D. C. Sayle, W. T. Self and S. Seal, The induction of angiogenesis by cerium oxide nanoparticles through the modulation of oxygen in intracellular environments, *Biomaterials*, 2012, **33**, 7746.

7 A. Dhall and W. Self, Cerium Oxide Nanoparticles: A Brief Review of Their Synthesis Methods and Biomedical Applications, *Antioxidants*, 2018, **7**, 97.

8 A. Pinna, C. Figus, B. Lasio, M. Piccinini, L. Malfatti and P. Innocenzi, Release of ceria nanoparticles grafted on hybrid organic–inorganic films for biomedical application, *ACS Appl. Mater. Interfaces*, 2012, **4**, 3916.

9 J. Colon, N. Hsieha, A. Fergusona, P. Kupelian, S. Seal, D. W. Jenkins and C. H. Baker, Cerium oxide nanoparticles protect gastrointestinal epithelium from radiation-induced damage by reduction of reactive oxygen species and upregulation of superoxide dismutase 2, *Nanomedicine*, 2010, **6**, 698.

10 G. A. Silva, Seeing the benefits of ceria, *Nature Nanotechnol.*, 2006, **1**, 92.

11 C. Xu and X. Qu, Cerium oxide nanoparticle: a remarkably versatile rare earth nanomaterial for biological applications, *NPG Asia Mater.*, 2014, **6**, e90.

12 F. Caputo, M. Mameli, A. Sienkiewicz, S. Licoccia, F. Stellacci, L. Ghibelli and E. Traversa, A novel synthetic approach of cerium oxide nanoparticles with improved biomedical activity, *Sci. Rep.*, 2017, **7**, 4636.

13 R. A. Yokel, S. Hussain, S. Garantziotis, P. Demokritou, V. Castranova and F. R. Cassee, The yin: an adverse health perspective of nanoceria: uptake, distribution, accumulation, and mechanisms of its toxicity, *Environ. Sci.: Nano*, 2014, **1**, 406.

14 H. J. Eom and J. Choi, Oxidative stress of CeO_2 nanoparticles *via* p38-Nrf-2 signaling pathway in human bronchial epithelial cell, Beas-2B, *Toxicol. Lett.*, 2009, **187**, 77.

15 M. T. Tseng, Q. Fu, G. K. Lorc, R. Fernandez-Botran, Z.-B. Deng, U. M. Graham, D. A. Butterfield, E. A. Grulke and R. A. Yokel, Persistent Hepatic Structural Alterations Following Nanoceria Vascular Infusion in the Rat, *Toxicol. Pathol.*, 2014, **42**, 984.

16 A. Pinna, B. Lasio, M. Piccinini, B. Marmiroli, H. Amenitsch, P. Falcaro, Y. Tokudome, L. Malfatti and P. Innocenzi, Ceria nanoparticles for the treatment of Parkinson-like diseases induced by chronic manganese intoxication, *ACS Appl. Mater. Interfaces*, 2013, **5**, 3168.

17 N. M. Zholobak, V. K. Ivanov, A. B. Shcherbakov, A. S. Shaporev, O. S. Polezhaeva, A. Y. Baranchikov, N. Y. Spivak and Y. D. Tretyakov, UV-shielding property, photocatalytic activity and photocytotoxicity of ceria colloid solutions, *J. Photochem. Photobiol., B*, 2011, **102**, 32.
18 H. Xiang and Y. Chen, Energy-Converting Nanomedicine, *Small*, 2019, **15**, 1805339.
19 A. S. Karakoti, N. A. Monteiro-Riviere, R. Aggarwal, J. P. Davis, R. J. Narayan, W. T. Self, J. McGinnis and S. Seal, Nanoceria as Antioxidant: Synthesis and Biomedical Applications, *JOM*, 2008, **60**, 33.
20 G. V. Andrievsky, V. I. Bruskov, A. A. Tykhomyrov and S. V. Gudkov, Peculiarities of the antioxidant and radioprotective effects of hydrated C_{60} fullerene nanostructures *in vitro* and *in vivo*, *Free Radicals Biol. Med.*, 2009, **47**, 786.
21 P. J. Krusic, E. Wasserman, P. N. Keizer, J. R. Morton and K. F. Preston, Radical reactions of C_{60}, *Science*, 1991, **254**, 1183.
22 A. Pinna, L. Malfatti, M. Piccinini, P. Falcaro and P. Innocenzi, Hybrid materials with an increased resistance to hard X-rays using fullerenes as radical sponges, *J. Synchrotron Radiat.*, 2012, **19**, 586.
23 F. Ariu, L. Bogliolo, A. Pinna, L. Malfatti, P. Innocenzi, L. Falchi, D. Bebbere and S. Ledda, Cerium oxide nanoparticles (CeO_2 NPs) improve the developmental competence of *in vitro*-matured prepubertal ovine oocytes, *Reprod., Fertil. Dev.*, 2017, **29**, 1046.
24 S. M. Hirst, A. S. Karakoti, R. D. Tyler, N. Sriranganathan, S. Seal and C. M. Reilly, Anti-inflammatory properties of cerium oxide nanoparticles, *Small*, 2009, **5**, 2848.
25 R. Partha and J. L. Conyers, Biomedical applications of functionalized fullerene-based nanomaterials, *Int. J. Nanomed.*, 2009, **4**, 261.
26 N. Gharbi, M. Pressac, M. Hadchouel, H. Szwarc, S. R. Wilson and F. Moussa, Fullerene is a powerful antioxidant *in vivo* with no acute or subacute toxicity, *Nano Lett.*, 2005, **5**, 2578.
27 P. Innocenzi, P. Falcaro, S. Schergna, M. Maggini, E. Menna, H. Amenitsch, J. A. A. Soler-Illia, D. Grosso and C. Sanchez, One-pot self-assembly of mesostructured silica films and membranes functionalised with fullerene derivatives, *J. Mater. Chem.*, 2004, **14**, 1838.
28 N. Thakur, P. Manna and J. Das, Synthesis and biomedical applications of nanoceria, a redox active nanoparticle, *J. Nanobiotechnol.*, 2019, **17**, 84.
29 I. Selestin Raja, N. Duraipandi, M. S. Kiran and N. N. Fathima, An emulsion of pigmented nanoceria as a medicinal cosmetic, *RSC Adv.*, 2016, **6**, 100916.
30 I. Kalashnikova, J. Mazar, C. J. Neal, A. Rosado, S. Das, T. Westmoreland and S. Seal, Nanoparticle Delivery of Curcumin Induces Cellular Hypoxia and ROS-mediated Apoptosis *via* Modulation of Bcl-2/Bax in Human Neuroblastoma, *Nanoscale*, 2017, **9**, 10375.
31 T. Li, Z. Si, L. Hu, H. Qi and M. Yang, Prussian Blue-functionalized ceria nanoparticles as label for ultrasensitive detection of tumor necrosis factor-α, *Sens. Actuators, B*, 2012, **171–172**, 1060.
32 A. Pinna, L. Malfatti, G. Galleri, R. Manetti, S. Cossu, G. Rocchitta, R. Migheli, P. A. Serra and P. Innocenzi, Ceria nanoparticles for the treatment of Parkinson-like diseases induced by chronic manganese intoxication, *RSC Adv.*, 2015, **5**, 20432.
33 P. Sridharan, G. Vinothkumar, P. Pratheesh and K. S. Babu, Modulation of biomimetic properties of cerium oxide nanoparticles by hypoxic tumor microenvironments: steering towards tumor specificity, *New J. Chem.*, 2018, **42**, 6370.
34 J. T. Miller and D. E. Irish, Can, Infrared and Raman spectra of the cerium(IV) ion–nitrate ion–water system, *J. Chem.*, 1967, **45**, 147.
35 I. Kosack, V. Petrovsky, M. Anderson and P. Colomban, Raman Spectroscopy of Nanocrystalline Ceria and Zirconia Thin Films, *J. Am. Ceram. Soc.*, 2002, **85**, 2646.
36 W. Zhang, X. Gong, C. Liu, Y. Piao, Y. Sun and G. Diao, Water-soluble inclusion complex of fullerene with γ-cyclodextrin polymer for photodynamic therapy, *J. Mater. Chem. B*, 2014, **2**, 5107.
37 X. Zhang, Y. Huang, Y. Wang, Y. Ma, Z. Liu and Y. Chen, Global Atmospheric Emissions of Polycyclic Aromatic Hydrocarbons from 1960 to 2008 and Future Predictions, *Carbon*, 2008, **47**, 313.
38 B. M. Ginzburg, S. Tuœchiev, S. K. Tabarov, A. A. Shepelevskiœ and L. A. Shibaev, X-ray Diffraction Analysis of C_{60} Fullerene Powder and Fullerene Soot, *Tech. Phys.*, 2005, **11**, 1458.
39 A. Cid, Ó. A. Moldes, M. S. Diniz, B. Rodríguez-Gonzalez and J. C. Mejuto, Redispersion and Self-Assembly of C_{60} Fullerene in Water and Toluene, *ACS Omega*, 2017, **2**, 2368.
40 A. Kotani, T. Jo and J. C. Parlebas, Many-body effects in core-level spectroscopy of rare-earth compounds, *Adv. Phys.*, 1988, **37**, 37.
41 P. A. Connor, X. Yue, C. D. Savaniu, R. Price, G. Triantafyllou, M. Cassidy, G. Kerherve, D. J. Payne, R. C. Maher, L. F. Cohen, R. I. Tomov, B. A. Glowacki, R. V. Kumar and J. T. S. Irvine, Tailoring SOFC Electrode Microstructures for Improved Performance, *Adv. Energy Mater.*, 2018, **8**, 1800120.
42 R. C. Maher, G. Kerherve, D. J. Payne, X. Yue, P. A. Connor, J. Irvine and L. F. Cohen, The Reduction Properties of M-Doped (M = Zr, Gd) CeO_2/YSZ Scaffolds Co-Infiltrated With Nickel, *Energy Technol.*, 2018, **6**, 1.
43 A. Pfau and K. D. Schierbaum, Electronic structure of stoichiometric and reduced CeO_2 surfaces: An XPS UPS and HREELS study, *Surf. Sci.*, 1994, **321**, 71.
44 S. Barkam, S. Das, S. Saraf, R. Mc Cormack, D. Richardson, L. Atencio, V. Moosavifazel and S. Seal, The Change in Antioxidant Properties of Dextran-Coated Redox Active Nanoparticles Due to Synergetic Photoreduction–Oxidation, *Chem.–Eur. J.*, 2015, **21**, 12646.
45 P. Janoš, J. Henych, J. Pfeifer, N. Zemanová, V. Pilařová, D. Milde, T. Opletal, J. Tolasz, M. Malýd and V. Štengl, Nanocrystalline cerium oxide prepared from a carbonate

precursor and its ability to breakdown biologically relevant organophosphates, *Environ. Sci.: Nano*, 2017, **4**, 1283.
46 C. T. Campbell and C. H. Peden, Oxygen vacancies and catalysis on ceria surfaces, *Science*, 2005, **309**, 713.
47 L. Kundakovic, D. R. Mullins and S. H. Overbury, Adsorption and reaction of H_2O and CO on oxidized and reduced Rh/CeOx(111) surfaces, *Surf. Sci.*, 2000, **457**, 51.
48 J. Seo, J. Moona, J. H. Kima, K. Lee, J. Hwanga, H. Yoona, D. K. Yid and U. Paika, Role of the oxidation state of cerium on the ceria surfaces for silicate adsorption, *Appl. Surf. Sci.*, 2016, **389**, 311.
49 K. Mathrmool, A. Akkarapongtrakul, S. Sukkum and T. Bongkarn, Low Temperature Fabrication of Lead-Free KNN-BNT Ceramics *via* the Combustion Technique, *Ferroelectrics*, 2014, **458**, 136.
50 W. Deng, D. Chen, J. Hu and L. Chen, A general and green approach to synthesize monodisperse ceria hollow spheres with enhanced photocatalytic activity, *RSC Adv.*, 2015, **98**, 80158.
51 Y. Xu, N. Gao, Y. Gong, S. Huo, M. M. Mohideen, S. Hong and Y. Liu, Controllable preparation of methyltriethoxysilane xerogel nanofibers, *J. Mater. Sci.*, 2019, **54**, 10130.
52 R. Czochara, J. Kusio and G. Litwinienko, Fullerene C_{60} conjugated with phenols as new hybrid antioxidants to improve the oxidative stability of polymers at elevated temperatures, *RSC Adv.*, 2017, **70**, 44021.
53 S. Leach, M. Vervloet, A. Desprès, E. Bréheret, J. P. Hare, T. J. Dennis, H. W. Kroto, R. Taylor and D. R. W. Walton, Electronic spectra and transitions of the fullerene C_{60}, *Chem. Phys.*, 1992, **160**, 451.
54 R. Signorini, M. Meneghetti, R. Bozio, M. Maggini, G. Scorrano, M. Prato, G. Brusatin, P. Innocenzi and M. Guglielmi, Optical limiting and nonlinear optical properties of fullerene derivatives embedded in hybrid sol–gel glasses, *Carbon*, 2000, **38**, 1653.
55 K. I. Maslakova, Y. A. Teterin, A. J. Popel, A. Y. Teterin, K. E. Ivanov, S. N. Kalmykov, V. G. Petrov, P. K. Petrov and I. Farnan, XPS study of ion irradiated and unirradiated CeO_2 bulk and thin film samples, *Appl. Surf. Sci.*, 2018, **448**, 154.
56 T. S. Wu, L. Y. Syu, C. N. Lin, B. H. Lin, Y. H. Liao, S. C. Weng, Y. J. Huang, H. T. Jeng, S. Y. Lu, S. L. Chang and Y. L. Soo, Enhancement of catalytic activity by UV-light irradiation in CeO_2 nanocrystals, *Sci. Rep.*, 2019, **9**, 8018.
57 J.-H. Maeng and S.-C. Choi, The Effect of Cerium Reduction on Light Emission in Cerium-containing $20Y_2O_3$–$25Al_2O_3$–$55SiO_2$ Glass, *J. Opt. Soc. Korea*, 2012, **16**, 414.
58 A. Bianco, F. Gasparini, M. Maggini, D. Misiti, A. Polese, M. Prato, G. Scorrano, C. Toniolo and C. Villani, Molecular Recognition by a Silica-Bound Fullerene Derivative, *J. Am. Chem. Soc.*, 1997, **119**, 7550.

